Journal of Materials Chemistry A

ROYAL SOCIETY OF CHEMISTRY

REVIEW

View Article Online
View Journal

Cite this: DOI: 10.1039/d6ta00964f

Polyamines with reactive CO_2 diffusion for carbon capture: the obvious and the unexpected

Shweta Singh, † Taliehsadat Alebrahim,† Narjes Esmaeili, Yang Jiao* and Haiqing Lin *

Polyamines have emerged as a leading materials platform for sorbents in direct air capture (DAC) of CO_2 and membranes for post-combustion capture (PCC) due to their reactions with CO_2. Such reactions compete with hydrogen bonding among amine groups, are sensitive to temperature and water content, and can self-limit the further diffusion and sorption of CO_2 in polyamines. These unique characteristics give rise to interesting, often conflicting phenomena in DAC sorbents and PCC membranes, which have not been resolved at the molecular level. Herein, we highlight the imbalanced effects of substrates on amine efficiency for CO_2 sorption, the complex interplay of temperature and time on pseudo-equilibrium CO_2 sorption, and the intricate effects of water vapor on CO_2 sorption and desorption in DAC. For PCC membranes, both facilitated and hindered CO_2 transport are critically reviewed with an integrated experimental and simulation approach. We elucidate the role of CO_2-reactive diffusion in both sorbent and membrane applications, providing cohesive guidance for designing polyamine-based systems to enhance CO_2 capture performance.

Received 31st January 2026
Accepted 27th April 2026

DOI: 10.1039/d6ta00964f

rsc.li/materials-a

1 Introduction

The use of abundant carbon-based energy sources (such as coal, natural gas, oil, and traditional biomass) has dramatically improved living conditions for our society, but it inevitably increases atmospheric CO_2 concentrations, influencing the global climate. These carbon-based energy sources are inexpensive, account for 80–90% of global energy consumption, and are expected to continue playing a significant role in the energy landscape due to their well-established infrastructure and reliability. Therefore, mitigating CO_2 emissions into the atmosphere has emerged as a grand challenge for our society.

Various approaches to carbon capture have been explored, and two have attracted significant attention for their potential impacts.[1] First, CO_2 can be captured from the air (*i.e.*, direct air capture, or DAC), thereby directly reducing atmospheric CO_2 concentration.[2–4] Such technologies can be used at any location and may be carbon-negative. To this end, solid sorbents are widely used for DAC, as they offer low energy input, low operating costs, and good scalability. Second, CO_2 can be captured from flue gas at various point sources after combustion of carbon sources (*i.e.*, post-combustion carbon capture, or PCC).[5–7] For instance, flue gas streams from coal-fired power plants contain 10–13% CO_2, 82% N_2, and other components such as O_2 and H_2O. As an add-on approach, it does not disrupt existing industrial or power plants and may significantly reduce CO_2 emissions, as these point sources account for ~40% of CO_2 emissions. To this end, membrane technology has emerged as one of the leading technologies due to its high energy efficiency, small footprint, and avoidance of chemical use and emission.[5,8–10]

Interestingly, polyamines have emerged as a leading materials platform for both DAC sorbents[11–14] and PCC membranes.[7,8,15,16] Amine groups are key to achieving high CO_2 sorption capacity and selectivity over the major components of air (N_2 and O_2).[17,18] Eqn (1) and (2) elucidate the reaction mechanisms for the reaction between primary and secondary amines and CO_2. Under dry conditions, these amines react with CO_2 to form ammonium carbamate.[19,20] The maximum molar ratio of CO_2/N can reach 0.5 and increase to 1.0 in the presence of moisture (forming bicarbonates), as shown in eqn (3). Eqn (4) also shows that tertiary amines can react with CO_2 at a 1 : 1 molar ratio in the presence of water vapor:

$$CO_2 + 2RNH_2 \leftrightarrow RNH_3^+ + RNHCOO^- \quad (1)$$

$$CO_2 + 2R_1R_2NH \leftrightarrow R_1R_2NH_2^+ + R_1R_2NCOO^- \quad (2)$$

$$CO_2 + R_1R_2NH + H_2O \leftrightarrow R_1R_2NH_2^+HCO_3^- \quad (3)$$

$$CO_2 + R_1R_2R_3N + H_2O \leftrightarrow R_1R_2R_3NH^+HCO_3^- \quad (4)$$

Separated review articles have been published on polyamines for DAC sorbents[12,21,22] and PCC membranes.[23] The effect of amine type and its structure (*e.g.*, tetraethylenepentamine (TEPA), polyethylenimine (PEI), and diethylenetriamine (DETA)) on CO_2 sorption performance has

Department of Chemical and Biological Engineering, University at Buffalo, The State University of New York, Buffalo, NY 14260, USA. E-mail: yjiao3@buffalo.edu; haiqingL@buffalo.edu

† Singh and Alebrahim: equal contribution.

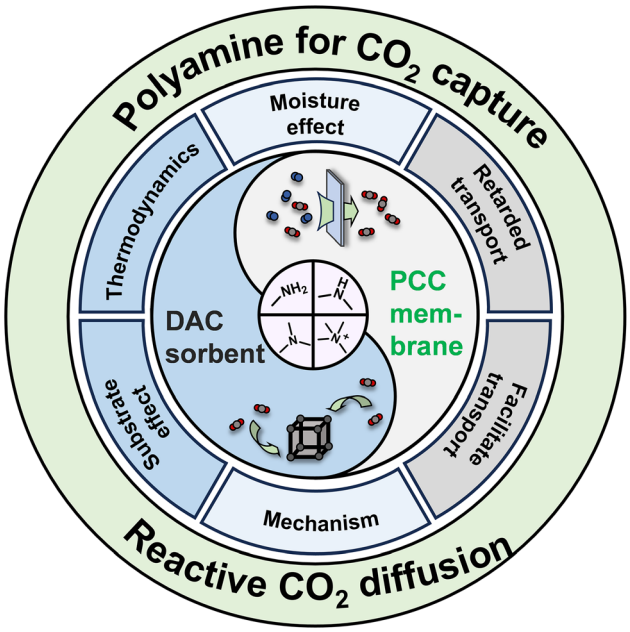

Fig. 1 Overview of polyamine-based sorbents for direct air capture (DAC) and membranes for post-combustion carbon capture (PCC: CO_2/N_2 separation).

also been reviewed in the literature.[21,22] In most cases, the affinity of amines for CO_2 was exploited to enhance CO_2 sorption and permeation, resulting in superior CO_2 separation performance. However, unusual phenomena have been reported in the literature: CO_2 sorption in polyamines increased with increasing temperature;[13,24,25] their affinity hindered CO_2 diffusion and reduced CO_2 permeability, resulting in unexpectedly high N_2/CO_2 and H_2/CO_2 selectivity.[26,27] These apparent contradictions in these two processes have not been resolved at the mechanistic level.

This paper highlights the unusual behaviors of polyamines for DAC sorbent and PCC membrane applications, underlying reactive CO_2 diffusion and its impact on CO_2 capture performance, and provides a cohesive framework for CO_2 transport in both sorbents and membranes (Fig. 1). First, we critically review polyamines on a broad spectrum of substrates for DAC and underline how substrates affect reactive CO_2 diffusion and sorption in these sorbents. The effect of water vapor, temperature, and time on CO_2 capture capability is revealed. Second, polyamine-based membranes for PCC are discussed, and the facilitated and hindered transport mechanisms are elucidated and contrasted through modeling and experiments. Finally, the contradictory results are analyzed to emphasize CO_2 reactive diffusion in polyamines, shedding light on the design of next-generation sorbents and membranes with enhanced carbon capture performance.

2 Polyamine-based sorbents for direct air capture

The key to DAC is high-performance sorbents with high CO_2 sorption capacity, long-term durability, and low costs.[12,28,29] Polyamines, such as polyethylenimine (PEI), have been widely used due to their strong interactions with CO_2, and they are often incorporated into porous supports to enhance the accessibility of amines to dilute CO_2 in air and to reduce pressure drops through the sorbents.[22,30–32]

The morphology of the support materials used to incorporate or append polyamines for DAC applications plays a significant role in determining carbon capture performance.[11,13] Support materials are selected based on key properties, including high surface area, appropriate pore size and pore structure, and good thermal and mechanical stability, as well as their interactions with polyamines. All these factors determine the distribution of polyamines (such as their layer thickness on the inner wall) and the structural characteristics of the resulting sorbents (such as pore size and porosity), thereby impacting CO_2 diffusion to amine sites and CO_2 sorption kinetics, including effects of diffusion resistance.[19,33] Notably, various approaches have been adopted to reduce diffusion limitations in these sorbents and enhance CO_2 accessibility to active amine sites, such as incorporating surfactants[34] and low viscosity diluents like polyethylene glycol (PEG)[35] and ionic liquids.[36] Additionally, supports with bimodal porous structures have been shown to facilitate rapid CO_2 diffusion while maintaining high amine loading.[37]

A variety of porous materials suitable for amine impregnation have been explored for DAC applications, including silica, zeolites, polymeric porous substrates, and newly emerging microporous materials such as metal–organic frameworks (MOFs) and covalent organic frameworks (COFs). Table 1 lists representative polyamine sorbents, based on various substrates and amine structures (primary, secondary, and tertiary amines), along with their DAC properties. In general, it is difficult to directly compare the capture performance of the sorbents due to the complex interplay between the supports' pore morphologies and interactions with polyamines, and there is no quantitative analysis or prediction of the effect of the porous support on DAC properties, in addition to CO_2 binding strength and diffusion resistance. Therefore, instead of conducting a comprehensive review, we highlight representative sorbents with high CO_2 sorption capacities, particularly their unusual behaviors, including the effects of temperature and water vapor on DAC performance. Detailed mechanisms are also provided in Section 4. Discussion and conclusion.

2.1 Sorbents based on inorganic porous substrates

Porous silica supports, such as SBA-15, have been widely used to incorporate PEI for DAC applications. SBA-15 was further modified with hydrophobic vinyltrimethoxysilane (VTMS), as shown in Fig. 2a.[48] The modified support was then acid-etched to remove boron and hydrolyze the remaining methoxy groups, followed by impregnation with 20 wt% PEI. The generated hydroxyl groups had a good affinity towards PEI. Additionally, a hydrophobic agent, HMDS (hexamethyldisilazane), was also used to modify SBA-15, enhancing the surface morphology.

Fig. 2b illustrates how surface hydrophobicity affects PEI distribution on the support and amine efficiency of the

Table 1 Physical properties and DAC performance of representative sorbents based on polyamines. Gas mixtures contain 400 ppm CO_2 in air

Substrates		Polyamines						
Types	Names	Types[a]	Content (%)	Surface area ($m^2\ g^{-1}$)	Temp. (°C)	RH (%)	CO_2 sorption (mmol g^{-1})	Ref.
Silica	Silica	PEI	47	—	25	0	2.4	38
	HS	TEPA	70	—	30	0	5.2	39
	H–SiO_2	PEI	~70	—	30	19	3.4	40
	γ-Alumina	PEI	48.1	—	25	0	1.7	41
	γ-Al_2O_3	TEPA	20	—	−20	0	0.81	42
		PEI	40	—	25	70	2	
	SBA-15	TEPA	—	500–800	25	0	1.5–2.5	43
		LPPI	50	80	25	0	1.2	44
		PPI	40	—	35	0	1.4	45
		PEI	39.9		25	0	1.1	41
		Ph-3-ED	60	—	35	0	1.9	46
					35	30	2.9	
		Ph-3-PD	50	55	35	0	0.56	
		AEAPTMS	—	45	25	0	1.7	47
	V-B-SBA-15	PEI	20	600–900	25	40	2.5–3	48
	Ti-SBA-15	PEI	31.8	209	25	0	0.64	49
	Zr-SBA-15	PEI	34.7	230	25	0	0.85	49
	Mg/Al-MMO	PEI	67	—	25	0	2.3	50
		TEPA	67		25	0	3.0	51
	Titania-silsesquioxane aerogel	APTES	—	—	30	0	1.6	52
Porous polymers	Solupor	PEI	48	—	25	0	0.53	13
		PEI	48	—	25	30	1.3	
	PIM-1 (powder)	PEI	21	220	35	—	0.23	53
	PIM-1 (fibers)	PEI	25	30	35	—	0.25	
	PF-15	TAEA	21	8	25	50	1.0	54
	NFC	AEAPDMS	50	7.1	25	40	1.4	55 and 56
	Ion exchange resin	Quaternary ammonium	—	800	23	0.5	0.98	57
MOFs	Mg_2(dobpdc)	MMEN	12	70	25	0	2.1	58
		EN		1253	25	0	2.8	59
	MIL-101(Cr)	TREN	45	—	25	0	2.8	60
		PEI	45	—	25	0	1.1	
	MIL101(Cr)/CA	TEPA	10	1247	−20	70	0.46	61
		PEI	10	1200	−20	70	0.66	
	MOF-808	PA	—	—	25	50	0.7	62
COFs	COF-999	PEI	—	—	25	75	2.1	63
	COF-609	TAPA	—	—	25	50	0.39	64
	COF-709	SH-bPEI	—	—	25	75	1.2	65
	PE-MCM-41	Triamine	—	367	25	0	0.98	66
Hybrid materials	SIPs	PEI	49	—	25	0	3.7	67
		NPEI	49	—	25	0	2.8	67
	PAN/OPZN	NIPEI	—	—	25	0	1.7	68
	Li-SX zeolite	—	—	>600	25	0	1.3	69

[a] Ph-3-ED: phenyl-3-ethylene diamine; Ph-3-PD: phenyl-3-propylenediamine; PPI: branched poly(propylenimine); AEAPTMS: *N*-(3-(trimethoxysilyl) propyl)ethane-1,2-diamine; APTES: 3-aminopropyltriethoxysilane; NFC: nanofibrillated cellulose; TREN: tris(2-aminoethyl)amine; TEPA: tetraethylenepentamine; TAPA: tris(3-aminopropyl)amine; TAEA: tris(2-aminoethyl)amine; SH-bPEI: sulfhydryl-grafted PEI; AEAPDMS: *N*-(2-aminoethyl)-3-aminopropylmethyldimethoxysilane; PIM-1: polymer of intrinsic microporosity; PF-15: fibers of amidoxime functionalized PIM-1.

sorbents. On untreated substrates, PEI showed strong affinity for the surface due to its strong hydrogen bonding with surface silanol groups; HMDS treatment reduced amine–silanol interactions, and the high PEI loading resulted in plug-like domains. By contrast, for VTMS-treated support (V-SBA-15), the vinyl groups exerted a caging effect, limiting PEI mobility and its interactions with silanol groups, thereby improving amine accessibility.

Fig. 2c shows water isotherms for the substrates alone to compare their hydrophobicity and better understand the distribution and interactions of PEI after impregnation. H-SBA-15 and V-SBA-15 exhibited low water uptake due to their hydrophobic surface, whereas the pristine SBA-15 and V-B-SBA-15 showed higher water uptake. Particularly, V-B-SBA-15 had silanol nests that promoted water condensation. When incorporating 20 wt% PEI, SBA-15, H-SBA-15, and V-SBA-15 showed

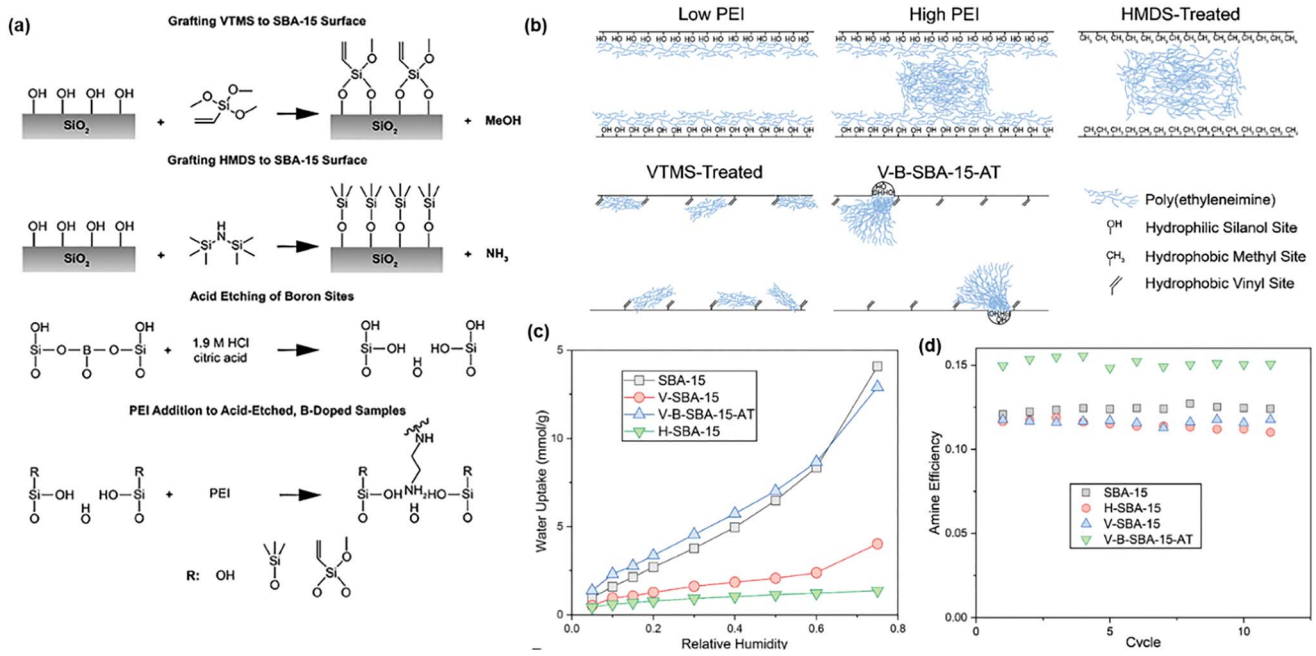

Fig. 2 PEI incorporated into SBA-15 modified using VTMS and HMDS. (a) Reaction scheme showing surface functionalization, acid etching of boron sites, and subsequent PEI incorporation. (b) Schematic illustration of porous supports with different PEI loadings and surface treatments. (c) Water sorption isotherms at 30 °C. (d) Amine efficiency at 40% RH and 400 ppm CO_2. Copyright 2024 Wiley.[48]

similar amine efficiency with 400 ppm CO_2 and 40% RH (Fig. 2d). By contrast, the V-B-SBA-15 showed 25% higher amine efficiency and good stability over 11 cycles. Additionally, H-SBA-15 showed degraded performance after 10 cycles due to its high hydrophobicity and the loss of PEI during thermal desorption.

2.2 Sorbents based on polymeric porous supports

Polymeric substrates have been used to prepare DAC sorbents due to their excellent processability, good handleability, and low costs, such as PIM-1 with microporosity and high surface area (>700 $m^2\ g^{-1}$).[54,70] Fig. 3a displays cellulose acetate hollow fibers containing MIL-101(Cr) (MIL-101(Cr)/CA), which were first spun *via* "dry-jet wet quench" process and then functionalized with polyamines such as tetraethylenepentamine (TEPA) and PEI *via* the wet impregnation method.[61] The fibers were porous, resulting in low pressure drops. Fig. 3b displays that the obtained sorbent exhibited a working capacity of 0.9 mmol g^{-1} during a temperature swing operation between −20 and 60 °C. The samples did not degrade throughout the 10 sorption/desorption cycles.

A commercial support, Solupor, made of high-density polyethylene (HDPE), was impregnated with branched PEI by wet impregnation (Fig. 3c).[13,71] Fig. 3d displays the effect of temperature and testing time on the sorption performance of a sorbent containing 48% PEI. Interestingly, increasing the temperature from 25 to 50 °C increased CO_2 pseudo-equilibrium sorption capacity by 36% from 0.53 to 0.72 mmol g^{-1} due to greater CO_2 diffusivity, which can be attributed to non-equilibrium CO_2 sorption caused by its self-restricted diffusion and pore blocking by PEI. As CO_2 reacts with PEI, it cross-links the PEI surface and lowers CO_2 diffusion (Fig. 3e). Increasing the temperature from 25 to 50 °C reduced the CO_2 content on the PEI surface and accelerated CO_2 diffusion into the films, enhancing CO_2 sorption. On the other hand, further increasing the temperature to 65 °C reduced CO_2 sorption capacity due to the dominant thermodynamic effect. The effect of diffusion-limited sorption has also been reported elsewhere.[24,25,72] For instance, increasing the temperature from −20 to 25 °C increased the sorption capacity by 70% from 1.26 to 2.14 mmol g^{-1} in 50 mass% TEPA-modified MIL-101(Cr).[73]

2.3 Sorbents based on MOFs

MOFs have emerged as a highly attractive platform for CO_2 capture due to their tunable pore structures, high surface areas, and thus high CO_2 sorption capacity.[74,75] Many MOFs containing open metal sites, such as MOF-74,[76] exhibit remarkable CO_2 uptake once guest molecules are removed from the framework. However, these materials often exhibit structural instability in the presence of water vapor, thereby reducing CO_2 sorption. Amine functionalization has been employed not only to enhance structural robustness but also to substantially improve CO_2 adsorption capacity through a moisture-assisted mechanism.

Fig. 4 compares the DAC performance of sorbents based on MIL-101(Cr) and a conventional γ-Al_2O_3 impregnated with TEPA.[11] Interestingly, MIL-101(Cr)-TEPA(30) showed weak chemisorption dominance (*i.e.*, CO_2 desorption occurred below 25 °C), while Al_2O_3-TEPA(20) showed strong chemisorption dominance (*i.e.*, CO_2 desorption occurred above 25 °C). Fig. 4a displays that MIL-101(Cr)_TEPA(30) mostly formed carbamic

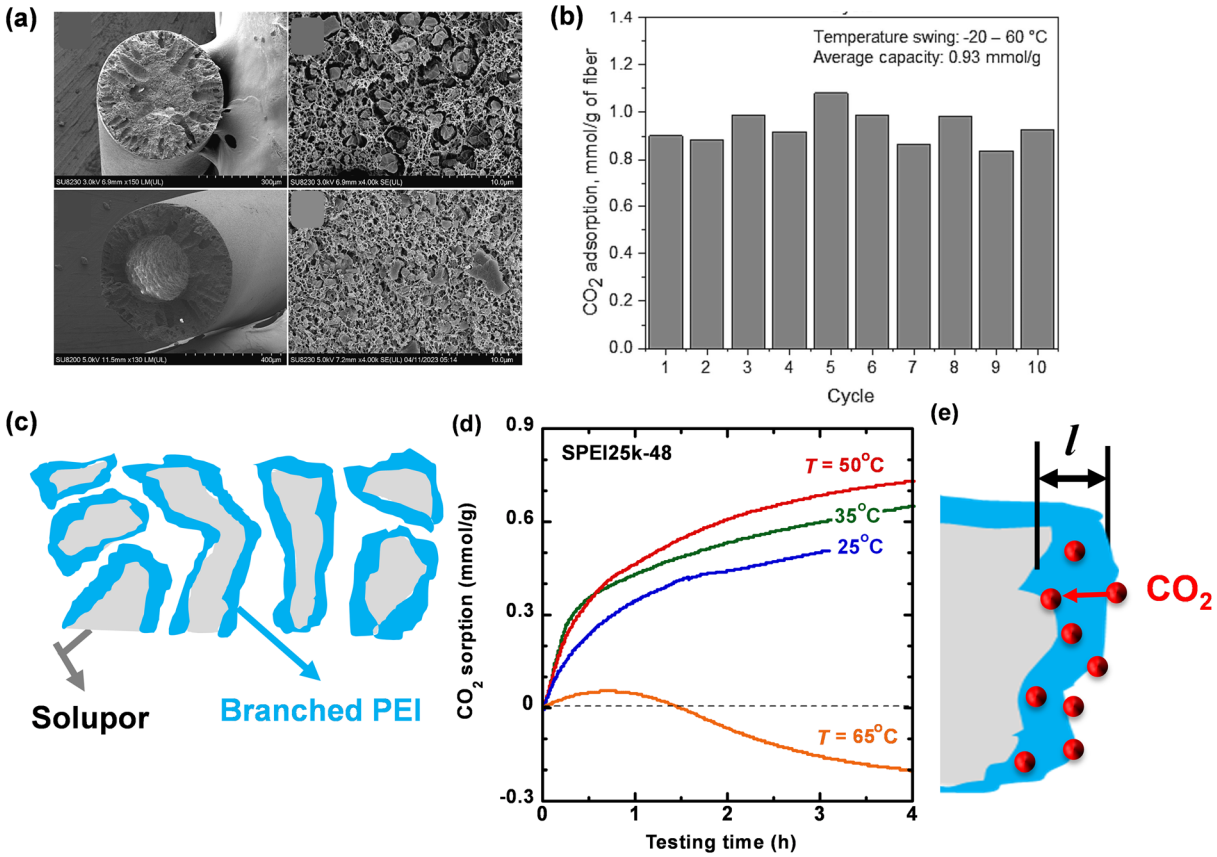

Fig. 3 Sorbents based on polymeric porous supports. (a) SEM images of dense and hollow MIL-101(Cr)/CA fibers; (b) PEI10 MIL-101(Cr)/CA fibers for TPD cycles under dry 400 ppm CO_2.[61] Copyright 2023 Elsevier. (c) PEI-incorporated Solupor (SPEI). (d) Effect of testing time and temperature on CO_2 sorption in the SPEI containing 48 mass% PEI (25k).[13] (e) Schematic of CO_2-reactive diffusion in PEI films. Copyright 2024 American Chemical Society.

acid with weak binding energy due to the strong amine-support interaction, along with a small amount of ammonium carbamate ion pairs, while Al_2O_3_TEPA(20) only formed ammonium carbamate with strong binding energy (Fig. 4b), which can be ascribed to the weak amine-support interactions and amine clustering. Nevertheless, there are no quantitative models in the literature for how support properties affect CO_2 binding strength under DAC conditions.[11,42,77]

Fig. 4c and d compares the effect of temperature and humidity on the sorption performance of MIL-101(Cr)_TEPA(30) and Al_2O_3-TEPA(20). Decreasing temperature increased the sorption capacity of MIL-101(Cr)_TEPA but decreased the capacity of Al_2O_3-TEPA, suggesting that the sorption in MIL-101(Cr)-TEPA was dominated by thermodynamic equilibrium, and the sorption in Al_2O_3-TEPA was limited by CO_2 diffusion into the bulk TEPA.

Fig. 5 demonstrates superior DAC performance by pip2-Mg_2(dobpdc) (pip2 = 1-(2-aminoehtly)piperidine).[78] Mg_2(dobpdc) containing diamines exhibited a maximum CO_2 uptake at a molar ratio of 1 for CO_2 : diamine; by contrast, pip2-Mg(dobpdc) exhibited a CO_2 : diamine ratio of 1.5 due to the cooperative chemisorption and physisorption steps.

Fig. 5b shows pure CO_2 adsorption isotherms with a two-step adsorption profile at 25, 40, and 50 °C, implying cooperative chemisorption and physisorption. At 25 and 40 °C, the first step of adsorption occurred at 50 and 150 mbar, yielding uptakes of 1.3 and 1.5 mmol g^{-1}, respectively. The second step showed a doubling of sorption capacity compared to the first step, yielding total capacities of 4.9 and 4.6 mmol g^{-1}, respectively. A similar increase in CO_2 uptake was observed at 50 °C; however, the uptake value was lower than that at lower temperatures. Fig. 5c shows the stability of pip2-Mg_2(dobpdc) over 500 cycles of adsorption–desorption, where the adsorption was conducted for 15 min with a dry CO_2/N_2 (60/40) mixture at 30 °C, and the desorption took place for 1 min under dry CO_2 at 80 °C. The sorbent demonstrated a consistent sorption capacity of 3.8 mmol g^{-1}.

2.4 Sorbents based on COFs

COFs have also been explored for CO_2 capture due to their pore structure and tunability, combining the structural advantages of MOFs with enhanced chemical and thermal stability enabled by covalent bonding.[79,80] Fig. 6a displays the synthesis of an amine-functionalized COF (COF-999), achieving high CO_2 sorption capacity, fast kinetics, and low regeneration energy.[63] Crystalline olefin-linked COF precursor (COF-999-N_3) was first synthesized, and then the azide group was converted to an amine group *via* the Staudinger reaction. The obtained COF-

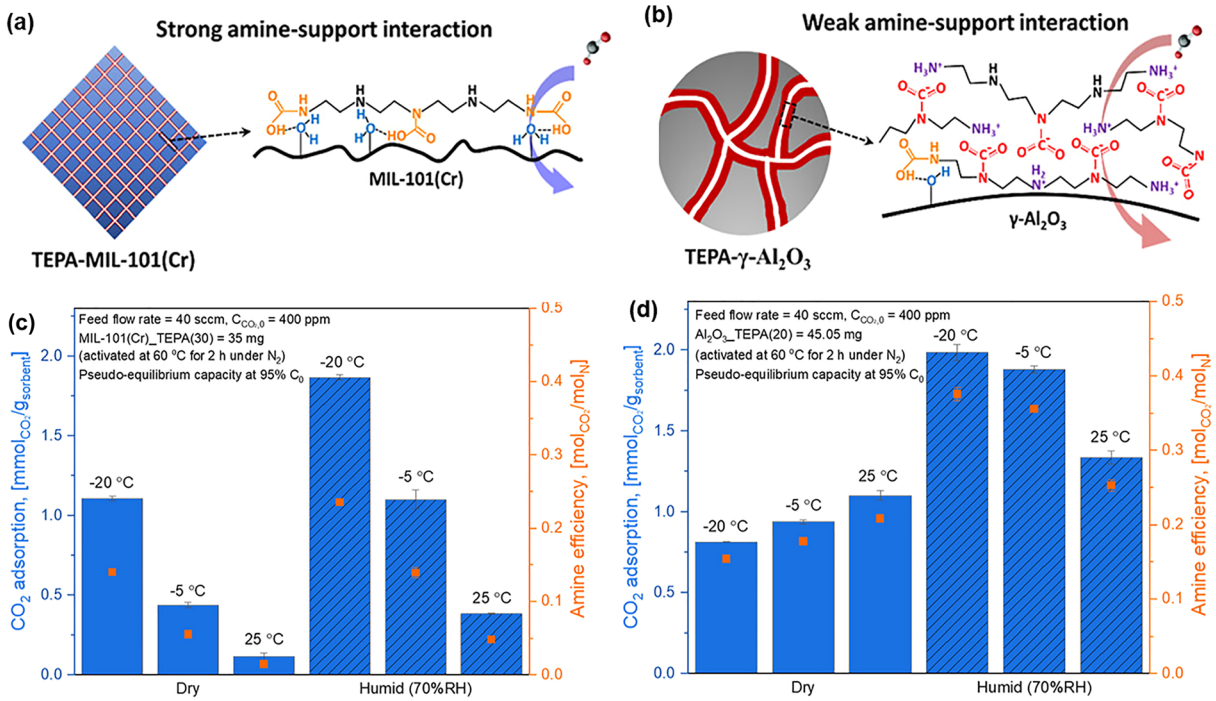

Fig. 4 Comparison of TEPA-containing sorbents based on γ-Al_2O_3 and MIL-101(Cr). Reaction mechanism of CO_2 with (a) γ-Al_2O_3_TEPA (with weak amine-support interaction) and (b) MIL-101(Cr)_TEPA (with strong amine-support interaction). Pseudo-equilibrium adsorption and amine efficiency of (c) MIL-101(Cr)_TEPA(30) and (d) γ-Al_2O_3_TEPA(20) at various temperatures under dry and humid (70% RH) conditions. Copyright 2023 American Chemical Society.[11]

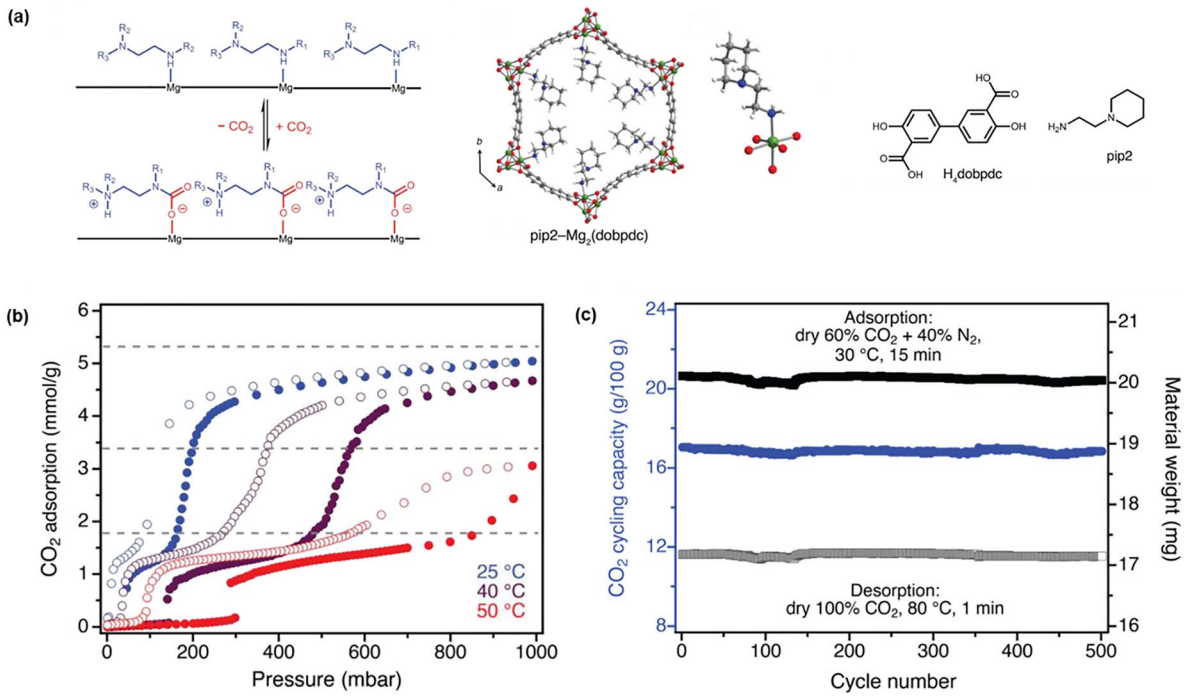

Fig. 5 Superior DAC performance by pip2-Mg_2(dobpdc). (a) (Left) CO_2 adsorption mechanism, (mid) simulated structure, and (right) H_4dobpdc and pip2 structures; (b) CO_2 sorption isotherms at 25, 40, and 50 °C. (c) Temperature-swing adsorption–desorption cycle at atmospheric pressure. Copyright (2024) American Chemical Society.[78]

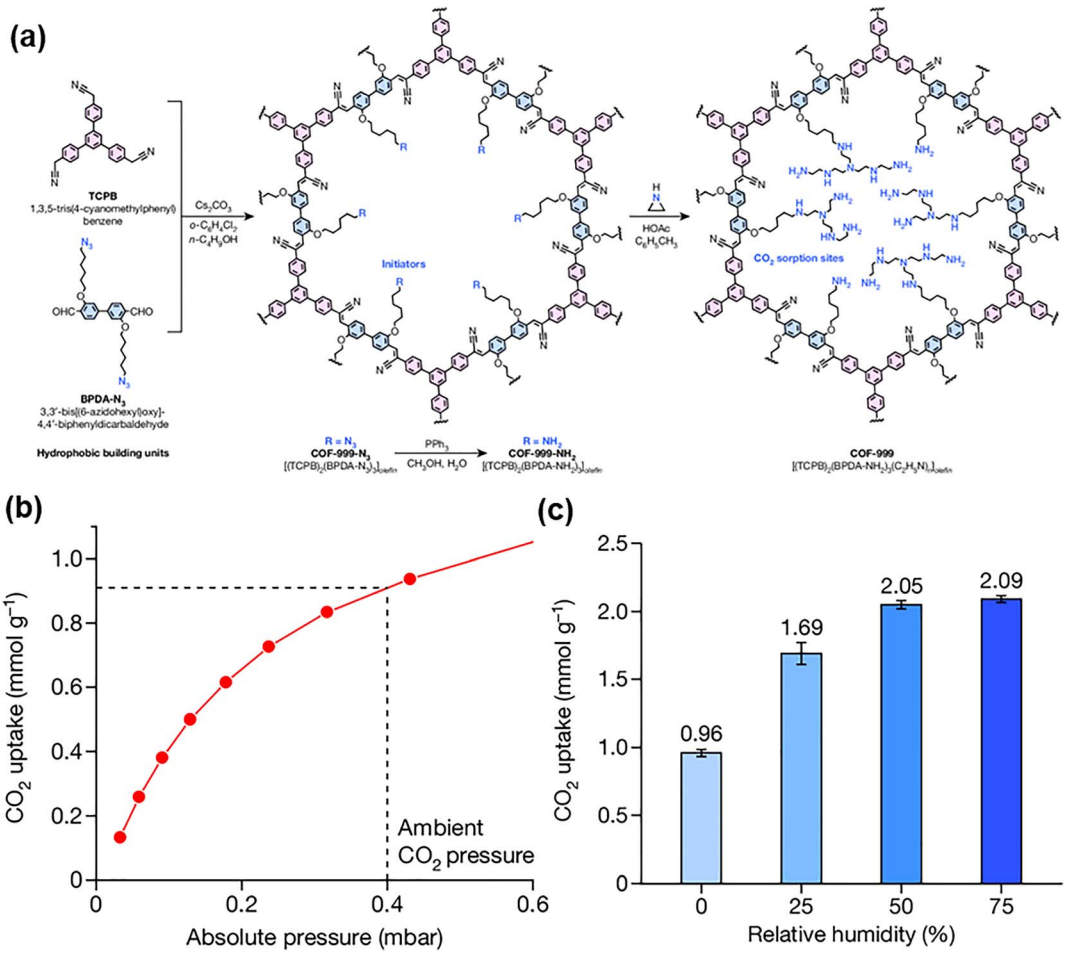

Fig. 6 DAC sorbent based on COF-999. (a) Schematic diagram of the material synthesis; (b) CO_2 sorption isotherm with 400 ppm CO_2; (c) CO_2 sorption uptake with RH values of 0%, 25%, 50% and 75% at 400 ppm CO_2. Copyright 2024 Springer Nature.[63]

999-NH_2 was further treated with aziridine to produce polyamines in the pores, ultimately yielding COF-999. Fig. 6b shows that COF-999 exhibited CO_2 uptake of 0.91 mmol g^{-1} with 400 ppm CO_2. The CO_2 sorption capacity increased with increasing RHs (Fig. 6c). The sorbent achieved a CO_2 sorption capacity of 2.09 mmol g^{-1} under 75% RH at 25 °C.

2.5 Sorbents based on hybrid liquid-nanoparticles

Hybrid materials have been developed for DAC sorbents using waterless CO_2 solvents, such as ionic liquids (ILs), CO_2-binding organic ligands, and liquid-like nanoparticle organic hybrid materials (NOHMs).[67] Fig. 7a shows that PEI-functionalized NOHMs (NOHM-I-PEI) can be encapsulated in a polymer shell by UV curing and formed into thin films. The solvent impregnated polymers (SIP) particles were synthesized by grinding these films, and the CO_2 capture mechanism of the NOHM-I-PEI-incorporated SIPs (NPEI-SIPs) is shown in Fig. 7a.

Fig. 7b compares the CO_2 capture kinetics of the hybrid material (NPEI-SIPs) containing 49% NOHM-I-PEI with that of the pristine NOHM-I-PEI. The NPEI-SIPs exhibited CO_2 sorption capacity of 5.55 mmol CO_2 per g NOHM-I-PEI, much higher than that for NOHM-I-PEI (0.09 mmol CO_2 per g). The base liquid exhibited high viscosity, resulting in very slow sorption kinetics; by contrast, the polymer matrix in the SIPs showed high CO_2 diffusivity, leading to fast kinetics. Fig. 7c shows that introducing water vapor (80% RH) increased CO_2 sorption capacity.

2.6 Moisture-driven DAC based on polyamine derivatives

Most polyamines are thermally regenerated after CO_2 sorption, leading to high energy consumption, and they are susceptible to oxidative degradation at high temperatures.[81,82] Recently, a novel approach of moisture-swing-based DAC has been developed with the sorbents regenerated at high RH and ambient temperature,[83–86] as shown in Fig. 8. These processes are often based on polyamine derivatives, such as quaternary ammonium-containing polymers. Specifically, CO_2 is captured under dry conditions and released upon exposure to higher RH levels, as shown in the equations in Fig. 8a. The hydroxide-functionalized quaternary ammonium groups react with CO_2 under dry conditions to form bicarbonate (eqn (i)). When exposed to high RH levels, water drives the reverse reaction, thereby converting bicarbonate to carbonate and releasing CO_2 (eqn (ii) and (iii)), enabling sorbent regeneration.

Fig. 8b displays the effect of RHs on CO_2 sorption in an example moisture-swing sorbent (fGO), prepared by functionalizing graphene oxide (GO) with glycidyltrimethylammonium

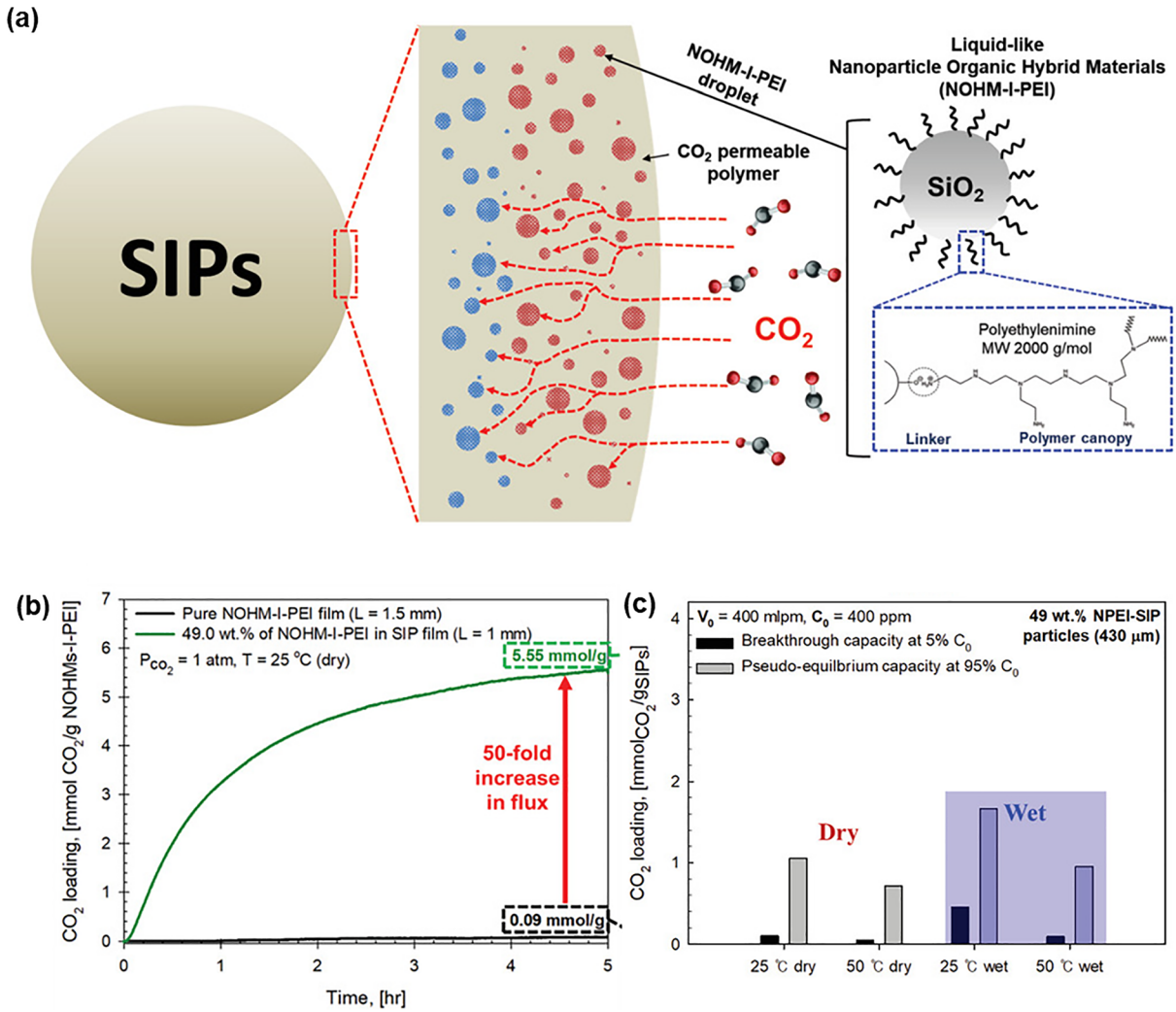

Fig. 7 CO_2 capture in NPEI-SIPs containing 49 mass% NOHM-1-PEI. (a) Structure and sorption mechanism. (b) Comparison with pristine NOHM-I-PEI. (c) Effect of humidity on CO_2 capture for 400 ppm CO_2.[67] Copyright 2021 Wiley.

chloride.[83] The fGO displayed the highest CO_2 uptake at 20% RH, followed by a decline in capacity as RH increased to 100%, giving a moisture-swing working capacity of 2.3 mmol g^{-1}. Moreover, the fGO sorbent exhibited excellent cycling stability, retaining performance for over 40 adsorption–desorption cycles, with only a 7.5% loss after 50 cycles.

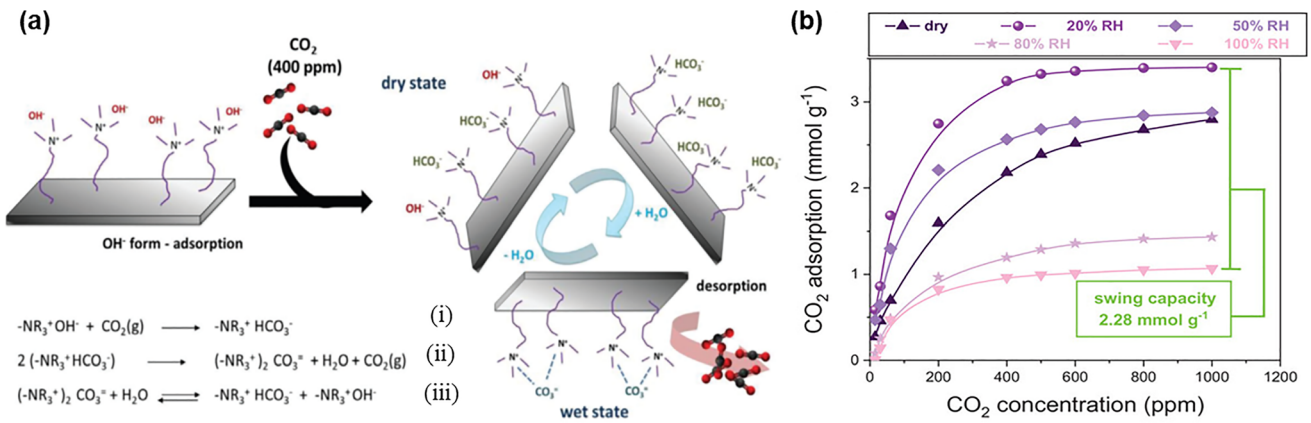

Fig. 8 Moisture-swing sorbents based on quaternary ammonium-functionalized graphene oxide (fGO). (a) Sorption and desorption mechanism, including three reactions, and (b) effect of humidity on CO_2 sorption.[83] Copyright 2024 Wiley.

3 Polyamines for membrane CO_2 separation

3.1 Modeling of facilitated CO_2 transport in polyamines

Gas transport in non-facilitated polymers is usually described using the solution-diffusion model, and gas permeability $\left(P_A,\ \text{Barrer},\ 10^{-10}\frac{\text{cm}^3(\text{STP})\text{cm}^{-1}}{\text{cm}^2\ \text{s}^{-1}\ \text{cm Hg}}\right)$ is expressed as:

$$P_A = S_A \times D_A \tag{5}$$

where S_A is the gas solubility, and D_A is the gas diffusivity. Gas permeance of a membrane $\left(Q_A,\ \text{GPU},\ 10^{-6}\frac{\text{cm}^3(\text{STP})}{\text{cm}^2\ \text{s}^{-1}\ \text{cm Hg}}\right)$ with a thickness (l, cm) is given by:

$$Q_A = P_A/l \tag{6}$$

Polyamines have been widely reported to facilitate CO_2 transport in the presence of water through reversible reactions with amines.[87,88] For example, in eqn (3), reagents and products can be simplified using the following abbreviations: A = CO_2, B = R–NH_2, C = HCO_3^-, and D = R–NH_3^+. Water solubility in polyamines is significantly larger than CO_2 solubility, and therefore, it is considered a constant.[89] The total amine concentration in polyamines (C_T) can be defined as follows:

$$C_T = C_B + C_D \tag{7}$$

The reaction equilibrium constant (K_{eq}) can be defined as:

$$K_{eq} = \frac{C_C C_D}{C_A C_B} \tag{8}$$

Assuming that the CO_2 partial pressure in the permeate is negligible, CO_2 flux (J_{CO_2}) can be calculated as follows:[90]

$$J_{CO_2} = \frac{D_A}{l}C_A^F + \frac{D_C}{l}C_C^F \tag{9}$$

where the superscript F indicates the properties in the feed. CO_2 concentration at the feed side (C_A^F) can be calculated using Henry's law: $C_A^F = H_A p_A^P$, where H_A is the Henry constant for CO_2.

HCO_3^- concentration can be correlated to the CO_2 concentration using eqn (7) and (8).

$$C_C^F = \frac{K_{eq}C_A}{2}\left(\sqrt{1+\frac{4C_T}{K_{eq}C_A^F}}-1\right) \tag{10}$$

By using eqn (9) and (10), CO_2 permeance (Q_{CO_2}) can be written as:[90]

$$Q_{CO_2} = \frac{J_{CO_2}}{p_A^F} = \frac{D_A H_A}{l} + \frac{D_C K_{eq} H_A}{2l}\left(\sqrt{1+\frac{4C_T}{K_{eq}H_A p_A^F}}-1\right) \tag{11}$$

where the 1st term on the right side of the equation describes Fickian diffusion, and the 2nd term accounts for the carrier-mediated diffusion for facilitated transport.

The physical properties parameters used in eqn (11) can be determined from CO_2 sorption isotherms. Additionally, a lumped form of eqn (7) was used to investigate the effect of CO_2 partial pressure on permeance, as follows.

$$\frac{Q_{CO_2}}{Q'_{CO_2}} = 1 + \eta\left(\sqrt{1+\frac{4C_T}{K_{eq}H_A p_A^F}}-1\right) \tag{12}$$

where Q'_{CO_2} is the permeance due to the solution-diffusion mechanism, and η represents the contribution of the facilitated transport. This facilitated transport model was validated using experimental data. As an example, eqn (12) agrees well with experimental CO_2 permeances as a function of CO_2 partial pressure (0.1–100 kPa) and operating temperatures (57–77 °C).[90]

To better understand the complex mechanism of facilitated transport, the role of amine carriers in these membranes was examined at the molecular level using computational approaches, including density functional theory (DFT) calculations and molecular simulations.[91–93] For example, DFT methods were utilized to investigate the amine-CO_2 chemistry of poly(*N*-vinylformamide-*co*-vinylamine) (PNVF-*co*-VAm) with fixed carriers and two mobile carriers, piperazine glycinate (PZ-Gly) and 2-(1-piperazinyl)ethylamine sarcosinate (PZEA-Sar) (Fig. 9a).[92] CO_2 interacts with amino groups *via* two primary reaction pathways: carbamate pathway (eqn (1) and (2)) and bicarbonate pathway (eqn (3) and (4)), in which the bicarbonate pathway with equimolar stoichiometry provides a higher CO_2 sorption capacity.

Fig. 9b displays that PZEA-Sar and PZ-Gly exhibited lower relative electronic energy ($\Delta E_{carbamate}$) values (−18.1 and −17.5 kcal mol^{-1}, respectively), compared to VAm (−13.8 kcal mol^{-1}) following the carbamate pathway, suggesting that CO_2 has a higher reactivity towards the primary amino group on the mobile carrier than the fixed carrier. The simulation results confirmed that adding PZEA-Sar to PNVF-*co*-VAm increased CO_2 permeance, with an increase greater than that observed with PZ-Gly. Furthermore, an MD simulation suggested that CO_2 diffused faster through the bicarbonate state than through the carbamate state, since bicarbonate species can not only associate with protonated carriers but also hop between them.[93] CO_2 reaction intermediates (carbamate and bicarbonate species) were also confirmed using *operando* surface-enhanced Raman spectroscopy (SERS) in combination with *in situ* transmission FTIR spectroscopy.[94]

3.2 Polyamine-based membranes with facilitated CO_2 transport

Amines can act as either fixed or mobile carriers within the polymer matrix. For fixed-carrier polyamines, the reactive amino groups are covalently bonded to the polymer backbone, in which CO_2 molecules can hop across amine reactive sites down the concentration gradient.[93,95,96] Alternatively, amine groups can be dispersed as small molecules within the polymer

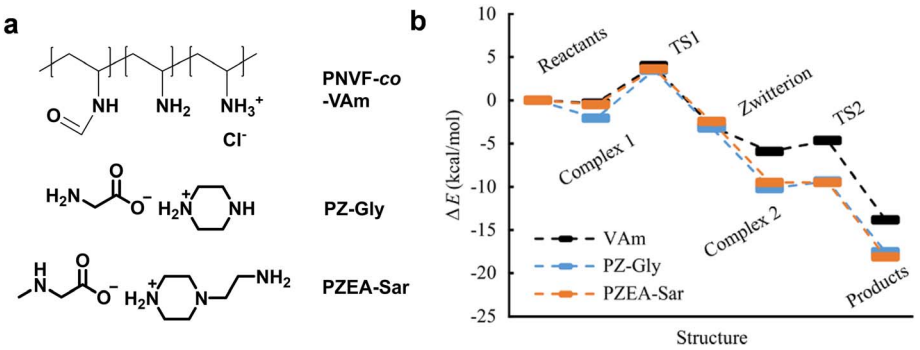

Fig. 9 DFT and MD calculation of facilitated CO_2 diffusion in PZ-Gly and PZEA-Sar. (a) Chemical structures. (b) Relative electronic energy ($\Delta E_{carbamate}$) of structures in the amine-CO_2 reactions of carriers. Copyright 2020 American Chemical Society.[92]

matrix, where they reversibly react with CO_2 and diffuse through the membrane, thereby enhancing CO_2 transport efficiency. Table 2 lists the representative polyamines and their CO_2/N_2 separation properties in water-saturated gas mixtures. In general, there is no correlation between the amine content and CO_2/gas separation properties,[97] while increasing water content typically increases CO_2 permeance and CO_2/gas selectivity.[98,99]

Fig. 10 illustrates the structure, composition, and CO_2/N_2 separation performance of polyamine-based TFC membranes.[8] Fig. 10a displays the configuration of membranes comprising a dense selective layer (~170 nm) supported on a porous support (30 μm). The selective layer contained both PNVF-*co*-VAm and PEGu as the fixed layer and PZEA-Sar as the mobile layer, which together provided a balance between CO_2 reactivity and structural integrity. Increasing the temperature from 67 to 77 °C increased CO_2 permeance from 2500 to 4200 GPU, accompanied by a slight decline in CO_2/N_2 selectivity. Additionally, PEI-decorated multilayered montmorillonite (MMT) was incorporated into PVAm membranes, resulting in CO_2 permeance of 217 GPU and CO_2/N_2 selectivity of 112.[111]

Fig. 11a shows a hybrid-integrated (HI) membrane comprising a modified amine-rich surface layer and a polymeric support layer with superior CO_2/N_2 separation properties.[7] Two commercial membranes, polydimethylsiloxane (PDMS) and polytetrafluoroethylene (PTFE AF), were selected as the support layer. The amine-functionalized PDMS and PTFE AF (am-PDMS and am-PTFE) exhibited lower CO_2 permeability than their pristine membranes, and CO_2 permeability decreased slightly with increasing pressure, consistent with the facilitated transport mechanism (Fig. 11b). By contrast, these membranes exhibited much higher mixed-gas CO_2/N_2 selectivity than their unmodified membranes (Fig. 11c). These membranes exhibited CO_2 permeability >1000 Barrer and CO_2/N_2 selectivity >100, surpassing the 2019 upper bound.[112]

Polyamines can also be used to fabricate porous materials (metal-induced ordered microporous polymers, or MMPs) for

Table 2 Representative polyamine-based facilitated transport membranes with CO_2 permeability (P_{CO_2}, Barrer) or permeance (Q_{CO_2}, GPU) and CO_2/N_2 selectivity with gas mixtures saturated by water

Polyamines[a]	Amine loading (wt%)	Thickness (μm)	Temp. (°C)	Pressure (bar)	CO_2 : N_2 mixture	Q_{CO_2}	P_{CO_2}	CO_2/N_2 selectivity	Ref.
PVAm		1.2	25	2	10 : 90	104		197	100
PG[b] (PVAm)	65	0.25	57	0.1	20 : 80	945		87	101
HMMP-1 (PVAm)	0.1	0.18	45	2	15 : 85	1544		252	102
PZEA-Sar/PEGu (PNVF-*co*-VAm)		0.17	67	4	20 : 80	2397		186	8
ProK (PVA)	40	0.5	≈23	2	10 : 90	791		40	103
UiO-66-NH_2 (*a*PEO)	10	0.328	23	2.36	15 : 85	1400		76	6
MMP-3		0.05	25	2	15 : 85	3000		78	104
am-PTFE AF		0.01	25	1.2	10 : 90		~1000	~1000	7
TMC/DNMDAm/DGBAmE		0.5	22	1.1	10 : 90		1613	138	105
PMVAm		12	102	1	20 : 80		6804	350	20
Lupamin® 9095/AIBA-K/AF-MWNT (PVA)	40	21	107	15	20 : 40		886	428	106
PAA-C_3H_7 (PVA)	70	25	110	2	20 : 40		295	335	88
NH_2–Co/ZIF-8 (PEO)	5	300	25	~0.1	10 : 90		2916	47	107
Porphyrin (PSF)	20		≈23	2–10	50 : 50		134	115	108
NUS-8-NH_2 (PIM-1)	10	54	25	2	20 : 80		14 638	29	109
UiO-66-NH_2@IL (PIM-1)	10	~70	20	1			8283	23	110

[a] The matrix is displayed in brackets. [b] PG: piperazine glycinate. PNVF-*co*-VAm: poly(*N*-vinylformamide-*co*-vinylamine); PEGu: poly(ethylene guanidine); PZEA-Sar: 2-(1-piperazinyl)ethylamine sarcosinate; ProK: potassium prolinate; PMVAM: poly(*N*-methyl-*N*-vinylamine); HMMP: high-valence MMP; MMP: metal-induced ordered microporous polymers; AIBA-K: 2-aminoisobutyric acid potassium salt.

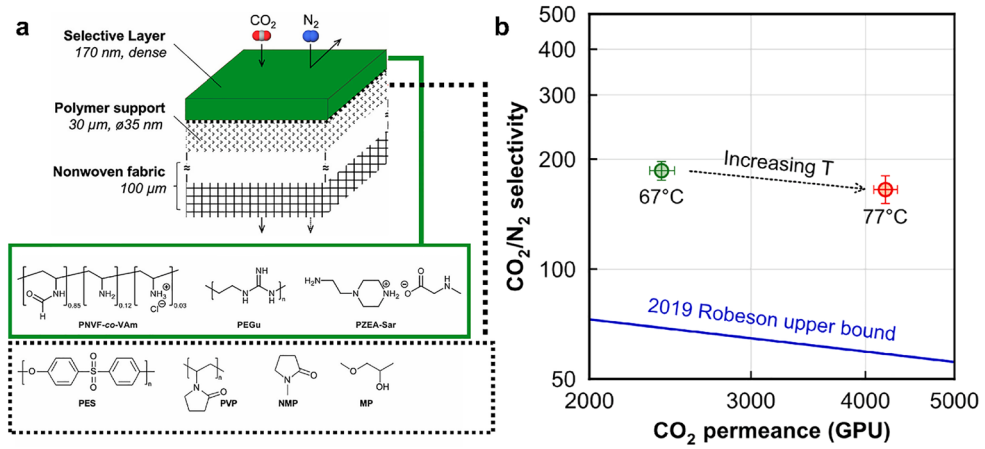

Fig. 10 Superior CO_2/N_2 separation performance in FTMs based on PNVF-*co*-VAm. (a) Schematic illustration and chemical composition, and (b) CO_2/N_2 separation performance of the scale-up membrane at 67 and 77 °C.[8] Copyright 2024 Elsevier.

CO_2/N_2 separation.[104] PVAm or PEI were selected as the amine-rich polymer, while aceclofenac or 4-chloroisophthalic acid served as small organic linkers, and $Cu(CH_3COO)_2$ or $Zn(NO_3)_2 \cdot 6H_2O$ as divalent metal ions (Fig. 12a). The Cl and carboxylate groups interacted with the polymer chains through dipolar interactions, forming the MMP structure (Fig. 12b). TFC membranes with a selective layer as thin as 50 nm on an mPSF support were fabricated over large areas (>100 cm^2) (Fig. 12c and d). The membrane exhibited a CO_2 permeance of 3000 GPU and CO_2/N_2 selectivity of 78 in the presence of saturated water vapor at 25 °C (Fig. 12e).

3.3 Polyamine-based membranes with hindered CO_2 transport

Although a variety of amine-modified polymers exhibit improved CO_2/N_2 selectivity under humidified conditions,

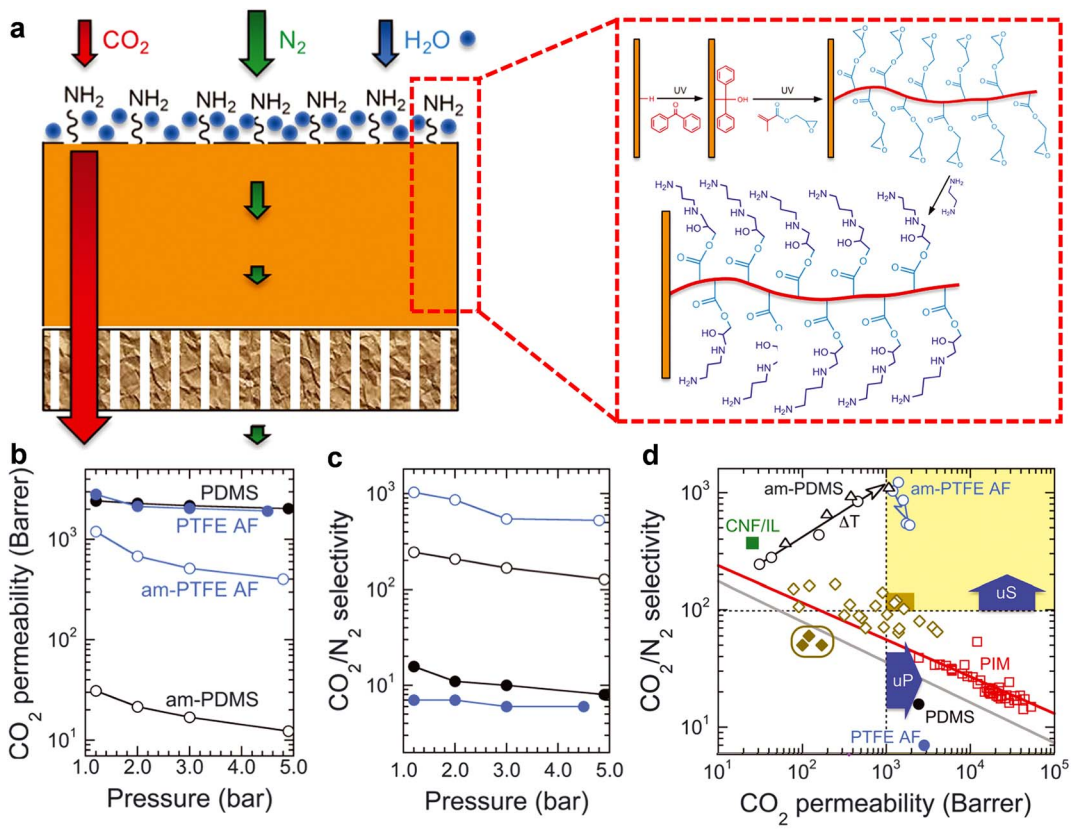

Fig. 11 Superior CO_2/N_2 separation properties in hybrid-integrated membranes of polymeric supports with amine-enriched surface. (a) Schematic. (b) CO_2 permeability and (c) CO_2/N_2 selectivity as a function of pressure. (d) Comparison with other polymers. The solid gray and red lines represent the 2008 (ref. 113) and 2019 upper bound,[112] respectively. Copyright 2022 AAAS.[7]

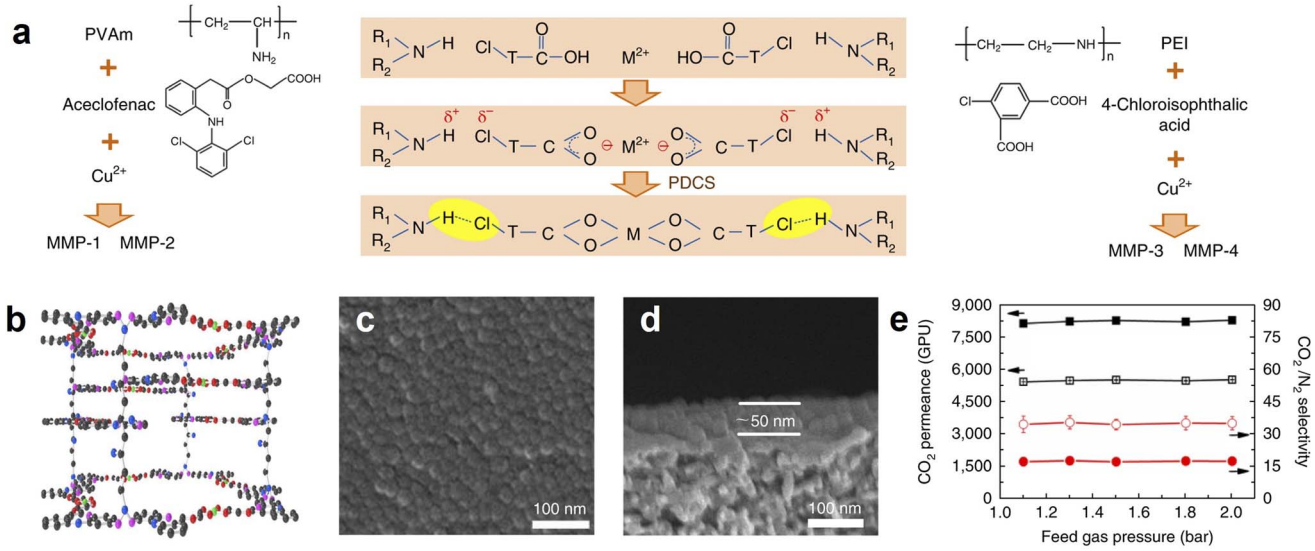

Fig. 12 Polyamine-derived MMP by the polymer-directed chemical synthesis (PDCS) strategy. (a) Schematic. (b) Independent frameworks of MMP-1. (c) Surface, (d) cross-section image, and (e) CO_2/N_2 separation performance of MMP-1/mPSf membrane. Filled and open points represent the mPSf and MMP/mPSf membrane, respectively. The feed gas was humid CO_2/N_2 mixed gas (v/v: 15/85) at 25 °C and 1–2 bar.[104] Copyright 2019 Springer Nature.

contradictory results have also been reported. For example, amine-functionalized polysulfone (PSF) was synthesized by introducing three basic substituents, namely arylamine, benzylamine, and phthalimide, leading to PSF-NH_2, PSF-CH_2–NH_2, and PSF-CH_2-imide, respectively (Fig. 13a).[114] Only PSF-CH_2–NH_2 showed enhancement in CO_2 solubility and CO_2/CH_4 solubility selectivity, and introducing arylamine and phthalimide diminished CO_2/CH_4 solubility selectivity (Fig. 13b and Table 3). For instance, PSF-NH_2 (38%) showed CO_2 solubility of 2.2 cm^3 (STP) (cm^{-3} atm^{-1}) and CO_2/CH_4 solubility selectivity of

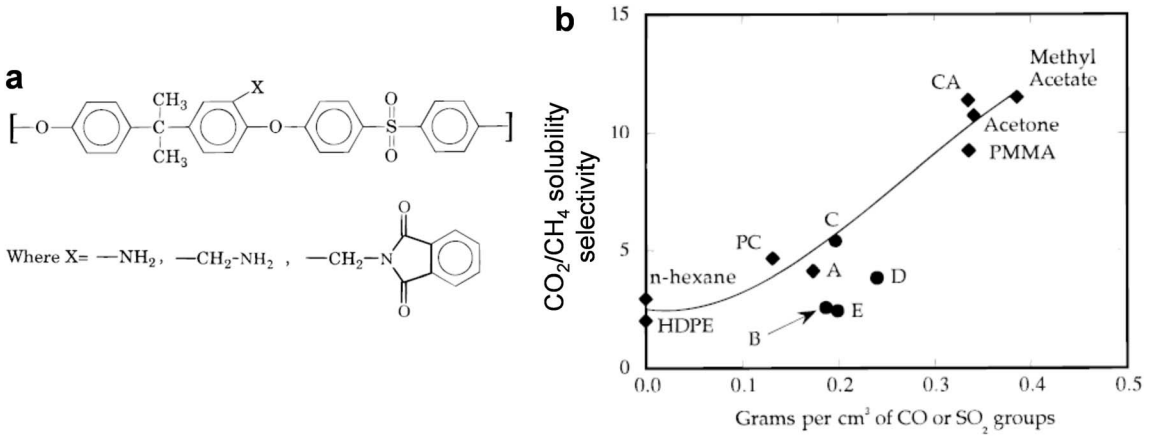

Fig. 13 Ineffective amine groups in amine-functionalized PSF. (a) Chemical structures. (b) Effect of polar group concentration on CO_2/CH_4 solubility selectivity. A = PSF, B = PSF-NH_2 (16%), C = PSF-NH_2 (51%), D = PSF-CH_2-imide (51%), and E = PSF-NH_2 (38%). Copyright 1996 American Chemical Society.[115]

Table 3 FFV and CO_2/CH_4 separation properties of the modified and unmodified PSF at 35 °C.[114,116] S_{CO_2} has a unit of cm^3 (STP) cm^{-3} atm^{-1}, and D_{CO_2} has a unit of 10^{-8} cm^2 s^{-1}

Polymers	FFV	S_{CO_2}	S_{CO_2}/S_{CH_4}	D_{CO_2}	D_{CO_2}/D_{CH_4}	P_{CO_2}(Barrer)	P_{CO_2}/P_{CH_4}
PSF	0.147	2.08	3.1	2.0	7.4	5.5	23
PSF-NH_2 (16%)	0.134	1.90	3.2	1.1	7.9	2.7	24
PSF-NH_2 (38%)	0.118	2.20	2.8	1.1	8.5	3.2	25
PSF-CH_2–NH_2 (51%)	0.125	3.04	4.7	0.5	3.5	1.95	18
PSF-CH_2 imide (51%)	0.122	1.76	3.4	0.9	7.6	2.12	26

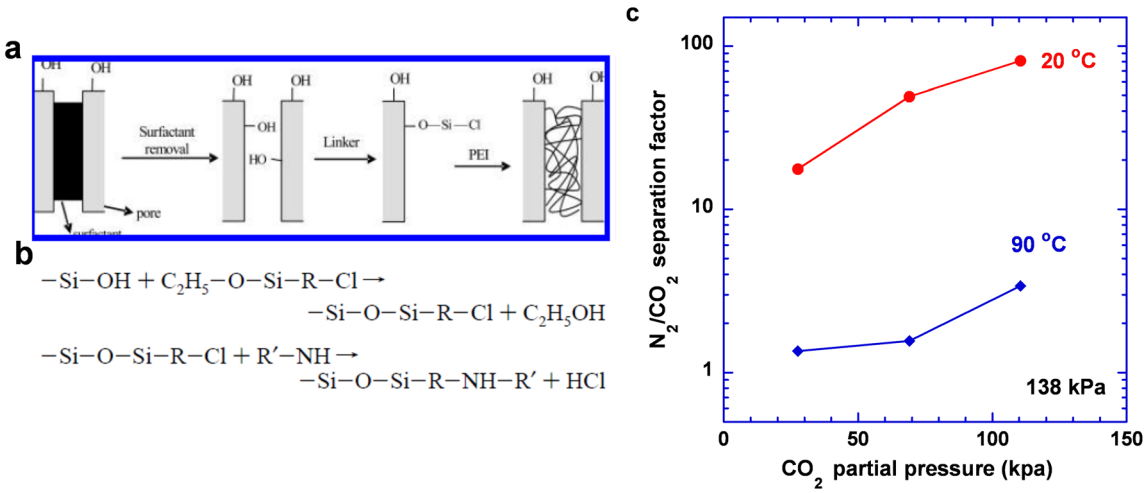

Fig. 14 Unexpectedly high N_2/CO_2 separation factor in HTMs based on PEI-modified MCM-48. (a) Membrane structure. (b) Reaction. (c) Effect of CO_2 partial pressure on N_2/CO_2 separation factor at 20 and 90 °C with 2.6% water vapor.[26] Copyright 2007 American Chemical Society.

2.8 at 35 °C, which were comparable to those of PSF (2.08 cm^3 (STP) (cm^{-3} atm^{-1}) and CO_2/CH_4 solubility selectivity of 3.1, respectively).

The amine functionalization decreased CO_2 diffusivity and thus permeability, which can be attributed to reduced fractional free volume (FFV). All amine-functionalized PSFs showed similar CO_2/CH_4 selectivity (Table 3), suggesting that amines interact with CO_2 with extremely low efficiency. Similarly, functionalization of PSF with tertiary amine groups (benzyldimethylamine or DMA) or quaternary ammonium groups did not enhance CO_2 solubility or CO_2/CH_4 solubility selectivity.[116]

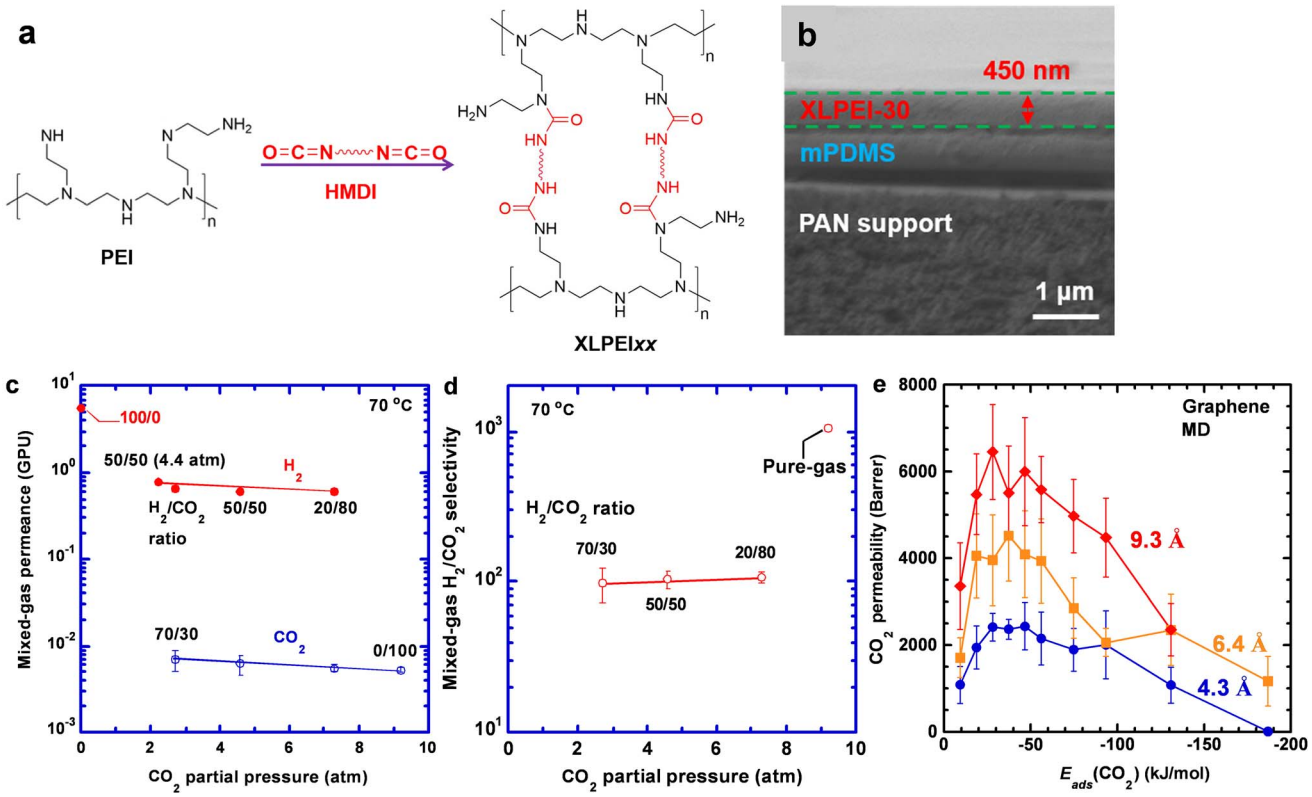

Fig. 15 Superior H_2/CO_2 separation performance of HTMs of XLPEI30.[27] (a) Synthesis of XLPEIs from PEI and HMDI. (b) Cross-sectional SEM image. (c) Mixed-gas permeance and (d) H_2/CO_2 selectivity as a function of the feed CO_2 partial pressure at 70 °C and 9 atm. (e) Mixed-gas CO_2 permeability as a function of CO_2 adsorption energy ($E_{ads}(CO_2)$) in simulated nanoporous graphene membranes with pore diameter from 4.3 to 9.3 Å. The error bars were calculated from ten replicate runs.

Fig. 14 presents another example of PEI-based hindered transport membranes (HTMs) with an unusual N_2/CO_2 separation factor.[26] A mesoporous MCM-48 membrane was impregnated with PEI, and the obtained membrane exhibited unexpectedly high N_2/CO_2 selectivity (18–81) at 20 °C, even in the presence of 2.6% water vapor, and the selectivity increased with increasing CO_2 concentration (or partial pressure) in the feed. By contrast, the membrane exhibited N_2/CO_2 separation factor of ~1 at 90 °C (Fig. 14c), which is still unexpected, considering the high content of amine groups in the membranes.

PEI can be cross-linked with hexamethylene diisocyanate (HMDI) at a 7 : 3 mass ratio (Fig. 15a) and used to form TFC membranes with a 450 nm-selective layer (XLPEI30, Fig. 15b).[27] Despite the high content of amine groups, the membrane exhibited H_2 permeance of 5.5 GPU and H_2/CO_2 selectivity of 1100, the highest reported for known polymeric membranes. The membrane was further evaluated with various H_2/CO_2 mixtures at 9.0 atm and 70 °C (Fig. 15c and d). The mixed-gas H_2 permeance was much lower than the pure-gas value (where CO_2 partial pressure is 0 atm) because of the ionic cross-linking of the XLPEI30 by the sorbed CO_2 during the mixed-gas permeation. Higher CO_2 partial pressure increased CO_2 sorption and cross-linking degree, decreased free volume, and decreased gas permeance, but retained mixed-gas H_2/CO_2 selectivity at 100.

Water vapor content plays an important role in determining H_2/CO_2 selectivity. Increasing relative humidity at 70 °C from 25% to 100% decreased H_2/CO_2 selectivity from 10 to 0.14.[27] To elucidate the hindered transport at the molecular level, CO_2 transport through a nanoporous graphene membrane was simulated using MD simulations (Fig. 15e), with adjustable CO_2 adsorption energies ($E_{ads}(CO_2)$) from −9.3 to −190 kJ mol^{-1} and pore diameters from 4.3 to 9.3 Å. CO_2 permeability initially increased with increasing $E_{ads}(CO_2)$ due to the enhanced affinity, but then decreased as the affinity became too strong for the sorbed CO_2 to desorb and diffuse through the membrane. Consequently, CO_2 permeability exhibited a volcano-shaped trend across all three pore sizes, with peaks at about −37 kJ mol^{-1}, indicating the boundary between CO_2-facilitated and hindered transport. Notably, this was only for dry conditions; when water vapor was introduced, it participated in the reaction between CO_2 and amines, facilitating CO_2 transport, decreasing H_2/CO_2 selectivity with increasing RH levels.

4 Discussion and conclusion

Polyamines with a strong affinity towards CO_2 have emerged as one of the most promising classes of materials for CO_2 capture, and their highly tunable molecular architecture has greatly expanded the design space for DAC sorbents and PCC membranes. As expected, polyamines react with CO_2, resulting in high CO_2 sorption capacity even at CO_2 levels as low as 400 ppm, and introducing water vapor further enhances CO_2 sorption capacity. However, several unusual, sometimes counterintuitive phenomena have been reported and are summarized below.

1. The amine efficiency towards CO_2 sorption depends sensitively on the substrates, and the measured pseudo-equilibrium CO_2 sorption may unconventionally increase with increasing temperature, reflecting the importance of the CO_2 diffusion and access of amine sites.

2. Polyamines can exhibit hindered CO_2 diffusion, leading to much lower CO_2 diffusivity than expected and unexpectedly high N_2/CO_2 or H_2/CO_2 selectivity. These results differ dramatically from those of FTMs, showing that CO_2 transport can be governed by reactive diffusion rather than a solution-diffusion mechanism.

3. The presence of water vapor influences CO_2 sorption and desorption, which has been harnessed to design moisture-swing sorbents and membranes for uphill CO_2 permeation based on polyamine derivatives.[84,85]

The key to understanding these discrepancies lies in the role of reactive CO_2 diffusion in polyamines.[93,117] As CO_2 diffuses through polyamines, it reacts with amines, forming ionic cross-links among polymer chains, increasing chain rigidity, reducing CO_2 diffusivity, and shielding the remaining polyamines from CO_2 access. However, no quantitative models are available to describe this behavior.[13,27] Furthermore, the strong interaction between CO_2 and amines may prevent the CO_2 dissociation and dramatically reduce its overall diffusivity. Consequently, the reported CO_2 sorption data are mostly at pseudo-equilibrium, and sorption is influenced by temperature thermodynamically and kinetically.

We expect that polyamines will remain a dominant materials platform for DAC sorbents and PCC membranes, and they may be optimized through integrated experimental and modeling studies. A key priority will be the creation of robust predictive frameworks that couple CO_2 sorption thermodynamics with mass-transfer kinetics, providing fundamental understanding of CO_2 reactive diffusion and facilitating scale-up from bench-top demonstration to commercial deployment.

Conflicts of interest

The authors declare no competing financial interests.

Data availability

Data are available upon request to the corresponding author.

Acknowledgements

We acknowledge the financial support of the U.S. Department of Energy National Energy Technology Laboratory (NETL # DE-FE0031960 and DE-SC0020730).

References

1 A. Ozden, M. Luo and Y. Lum, *Chem. Eng. J.*, 2025, **519**, 165535.
2 H. Akaya, S. Lamnini, H. Sehaqui and J. Jacquemin, *ACS Appl. Mater. Interfaces*, 2025, **17**, 16380–16395.

3 H. E. Holmes, M. J. Realff and R. P. Lively, *Nat. Chem. Eng.*, 2024, **1**, 208–215.
4 H. Bouaboula, J. Chaouki, Y. Belmabkhout and A. Zaabout, *Chem. Eng. J.*, 2024, **484**, 149411.
5 T. Merkel, R. Baker, P. Hao, J. Kniep, Z. He, Y. Huang and W. Salim, *J. Membr. Sci.*, 2026, **738**, 124829.
6 G. Zhang, C. J. Shah, W. I. Lee, K. Kisslinger, N. Esmaeili, V. T. Bui, L. Zhu, C. Y. Nam and H. Lin, *Adv. Funct. Mater.*, 2024, **34**, 2404785.
7 M. Sandru, E. M. Sandru, W. F. Ingram, J. Deng, P. M. Stenstad, L. Deng and R. J. Spontak, *Science*, 2022, **376**, 90–94.
8 Y. Yang, Y. Han, C. Zou, R. Pang, J. Hu, K. Chen and W. S. W. Ho, *J. Membr. Sci.*, 2024, **696**, 122520.
9 F. Attia, T. Tran, V. Bui, B. Valluri, E. Deng, G. Zhang, N. Esmaeili, L. Huang and H. Lin, *Chem. Mater.*, 2024, **36**, 9603–9612.
10 P. Ignatusha, H. Lin, N. Kapuscinsky, L. Scoles, W. Ma, B. Patarachao and N. Du, *Membranes*, 2024, **14**, 30.
11 G. Rim, P. Priyadarshini, M. Song, Y. Wang, A. Bai, M. J. Realff, R. P. Lively and C. W. Jones, *J. Am. Chem. Soc.*, 2023, **145**, 7190–7204.
12 X. Shi, H. Xiao, H. Azarabadi, J. Song, X. Wu, X. Chen and K. S. Lackner, *Angew. Chem., Int. Ed.*, 2020, **59**, 6984–7006.
13 T. Tran, S. Singh, S. Cheng and H. Lin, *ACS Appl. Mater. Interfaces*, 2024, **16**, 22715–22723.
14 Y. Jin, H. Lin, Y. Liu, H. An and J. Lee, *Renewable Sustainable Energy Rev.*, 2025, **217**, 115782.
15 S. Rao, Y. Han and W. W. Ho, *Sep. Sci. Technol.*, 2023, **58**, 1050–1071.
16 T. Tran, Y. Fu, D. Jiang and H. Lin, *Macromolecules*, 2022, **55**, 9860–9867.
17 A. A. Hosseini and M. J. Lashaki, *Sep. Purif. Technol.*, 2023, **325**, 124580.
18 J. Hack, N. Maeda and D. M. Meier, *ACS Omega*, 2022, **7**, 39520–39530.
19 E. S. Sanz-Perez, C. R. Murdock, S. A. Didas and C. W. Jones, *Chem. Rev.*, 2016, **116**, 11840–11876.
20 Z. Tong and W. S. W. Ho, *J. Membr. Sci.*, 2017, **543**, 202–211.
21 X. Shi, Y. Lin and X. Chen, *MRS Bull.*, 2022, **47**, 405–415.
22 A. Sayari, Q. Liu and P. Mishra, *ChemSusChem*, 2016, **9**, 2796–2803.
23 Y. Han and W. W. Ho, *J. Membr. Sci.*, 2021, **628**, 119244.
24 X. Wang, M. Fujii, X. Wang and C. Song, *Ind. Eng. Chem.*, 2020, **59**, 7267–7273.
25 X. Ma, X. Wang and C. Song, *J. Am. Chem. Soc.*, 2009, **131**, 5777–5783.
26 P. Kumar, S. Kim, J. Ida and V. V. Guliants, *Ind. Eng. Chem.*, 2008, **47**, 201–208.
27 L. Hu, A. J. Gottipalli, G. Zhang, K. Fung, T. Tran, N. Esmaeili, P. Zhang, Y. Ding, K. Shi and H. Lin, *Sci. Adv.*, 2025, **11**, eadz2830.
28 A. Sodiq, Y. Abdullatif, B. Aissa, A. Ostovar, N. Nassar, M. El-Naas and A. Amhamed, *Environ. Technol. Innov.*, 2022, **29**, 102991.
29 L. Jiang, W. Liu, R. Wang, A. Gonzalez-Diaz, M. Rojas-Michaga, S. Michailos, M. Pourkashanian, X. Zhang and C. Font-Palma, *Prog. Energy Combust. Sci.*, 2023, **95**, 101069.
30 A. Heydari-Gorji, Y. Yang and A. Sayari, *Energy Fuels*, 2011, **25**, 4206–4210.
31 A. Holewinski, M. A. Sakwa-Novak and C. W. Jones, *J. Am. Chem. Soc.*, 2015, **137**, 11749–11759.
32 H. Peng, J. Zhang, J. Zhang, F. Zhong, P. Wu, K. Huang, J. Fan and F. Liu, *Chem. Eng. J.*, 2019, **359**, 1159–1165.
33 L. A. Darunte, K. S. Walton, D. S. Sholl and C. W. Jones, *Curr. Opin. Chem. Eng.*, 2016, **12**, 82–90.
34 J. Wang, D. Long, H. Zhou, Q. Chen, X. Liu and L. Ling, *Energy Environ. Sci.*, 2012, **5**, 5742–5749.
35 L. Wang, M. Al-Aufi, C. N. Pacheco, L. Xie and R. M. Rioux, *ACS Sustain. Chem. Eng.*, 2019, **7**, 14785–14795.
36 J. Zhang, H. Peng, Y. Liu, D. Tao, P. Wu, J. Fan and K. Huang, *ACS Sustain. Chem. Eng.*, 2019, **7**, 9369–9377.
37 T. Witoon, *Mater. Chem. Phys.*, 2012, **137**, 235–245.
38 S. Choi, M. L. Gray and C. W. Jones, *ChemSusChem*, 2011, **4**, 628–635.
39 V. Kulkarni, D. Panda and S. K. Singh, *Ind. Eng. Chem.*, 2023, **62**, 3800–3811.
40 H. T. Kwon, M. A. Sakwa-Novak, S. H. Pang, A. R. Sujan, E. W. Ping and C. W. Jones, *Chem. Mater.*, 2019, **31**, 5229–5237.
41 W. Chaikittisilp, H.-J. Kim and C. W. Jones, *Energy Fuels*, 2011, **25**, 5528–5537.
42 P. Priyadarshini, G. Rim, C. Rosu, M. Song and C. W. Jones, *ACS Environ. Au*, 2023, **3**, 295–307.
43 A. Kumar, D. G. Madden, M. Lusi, K. Chen, E. A. Daniels, T. Curtin, J. J. Perry IV and M. J. Zaworotko, *Angew. Chem., Int. Ed.*, 2015, **54**, 14372–14377.
44 S. H. Pang, R. P. Lively and C. W. Jones, *ChemSusChem*, 2018, **11**, 2628–2637.
45 M. L. Sarazen, M. A. Sakwa-Novak, E. W. Ping and C. W. Jones, *ACS Sustain. Chem. Eng.*, 2019, **7**, 7338–7345.
46 D. R. Kumar, C. Rosu, A. R. Sujan, M. A. Sakwa-Novak, E. W. Ping and C. W. Jones, *ACS Sustain. Chem. Eng.*, 2020, **8**, 10971–10982.
47 S. Choi, J. H. Drese, P. M. Eisenberger and C. W. Jones, *Environ. Sci. Technol.*, 2011, **45**, 2420–2427.
48 A. Vallace, Z. S. Campbell, H. J. Moon, W. J. Koros, C. W. Jones and R. P. Lively, *Small*, 2024, **20**, 2401422.
49 Y. Kuwahara, D. Kang, J. R. Copeland, P. Bollini, C. Sievers, T. Kamegawa, H. Yamashita and C. W. Jones, *Chem.–Eur. J.*, 2012, **18**, 16649–16664.
50 X. Zhu, T. Ge, F. Yang, M. Lyu, C. Chen, D. O'Hare and R. Wang, *J. Mater. Chem. A*, 2020, **8**, 16421–16428.
51 M. Zhao, J. Xiao, W. Gao and Q. Wang, *J. Energy Chem.*, 2022, **68**, 401–410.
52 Y. Kong, G. Jiang, Y. Wu, S. Cui and X. Shen, *Chem. Eng. J.*, 2016, **306**, 362–368.
53 S. H. Pang, M. L. Jue, J. Leisen, C. W. Jones and R. P. Lively, *ACS Macro Lett.*, 2015, **4**, 1415–1419.
54 A. K. Sekizkardes, V. A. Kusuma, J. T. Culp, P. Muldoon, J. Hoffman, J. A. Steckel and D. Hopkinson, *J. Mater. Chem. A*, 2023, **11**, 11670–11674.

55 C. Gebald, J. A. Wurzbacher, P. Tingaut, T. Zimmermann and A. Steinfeld, *Environ. Sci. Technol.*, 2011, **45**, 9101–9108.
56 C. Gebald, J. A. Wurzbacher, A. Borgschulte, T. Zimmermann and A. Steinfeld, *Environ. Sci. Technol.*, 2014, **48**, 2497–2504.
57 T. Wang, K. S. Lackner and A. Wright, *Environ. Sci. Technol.*, 2011, **45**, 6670–6675.
58 T. M. McDonald, W. R. Lee, J. A. Mason, B. M. Wiers, C. S. Hong and J. R. Long, *J. Am. Chem. Soc.*, 2012, **134**, 7056–7065.
59 W. R. Lee, S. Y. Hwang, D. W. Ryu, K. S. Lim, S. S. Han, D. Moon, J. Choi and C. S. Hong, *Energy Environ. Sci.*, 2014, **7**, 744–751.
60 L. A. Darunte, A. D. Oetomo, K. S. Walton, D. S. Sholl and C. W. Jones, *ACS Sustain. Chem. Eng.*, 2016, **4**, 5761–5768.
61 M. Song, G. Rim, Y. Wang, I. Borne, C. W. Jones and R. P. Lively, *Chem. Eng. J.*, 2023, **477**, 147135.
62 O. I.-F. Chen, C. Liu, K. Wang, E. Borrego-Marin, H. Li, A. H. Alawadhi, J. A. Navarro and O. M. Yaghi, *J. Am. Chem. Soc.*, 2024, **146**, 2835–2844.
63 Z. Zhou, T. Ma, H. Zhang, S. Chheda, H. Li, K. Wang, S. Ehrling, R. Giovine, C. Li and A. H. Alawadhi, *Nature*, 2024, **635**, 96–101.
64 H. Lyu, H. Li, N. Hanikel, K. Wang and O. M. Yaghi, *J. Am. Chem. Soc.*, 2022, **144**, 12989–12995.
65 H. Li, Z. Zhou, T. Ma, K. Wang, H. Zhang, A. H. Alawadhi and O. M. Yaghi, *J. Am. Chem. Soc.*, 2024, **146**, 35486–35492.
66 Y. Belmabkhout, R. Serna-Guerrero and A. Sayari, *Ind. Eng. Chem. Res.*, 2010, **49**, 359–365.
67 G. Rim, T. G. Feric, T. Moore and A. H. A. Park, *Adv. Funct. Mater.*, 2021, **31**, 2010047.
68 K. D. Kersey, G. A. Lee, J. H. Xu, M. K. Kidder, A. H. A. Park and Y. L. Joo, *Adv. Funct. Mater.*, 2023, **33**, 2301649.
69 A. N. Stuckert and R. T. Yang, *Environ. Sci. Technol.*, 2011, **45**, 10257–10264.
70 K. Baamran, P. Muldoon, K. Damodaran, S. Banerjee, K.-J. Kim, J. A. Steckel and A. K. Sekizkardes, *Sep. Purif. Technol.*, 2025, 133186.
71 T. Tran, S. Pan, X. Chen, X.-C. Lin, A. K. Blevins, Y. Ding and H. Lin, *ACS Appl. Mater. Interfaces*, 2020, **12**, 49192–49199.
72 F. Rezaei, R. P. Lively, Y. Labreche, G. Chen, Y. Fan, W. J. Koros and C. W. Jones, *ACS Appl. Mater. Interfaces*, 2013, **5**, 3921–3931.
73 G. Rim, F. Kong, M. Song, C. Rosu, P. Priyadarshini, R. P. Lively and C. W. Jones, *JACS Au*, 2022, **2**, 380–393.
74 P. M. Bhatt, Y. Belmabkhout, A. Cadiau, K. Adil, O. Shekhah, A. Shkurenko, L. J. Barbour and M. Eddaoudi, *J. Am. Chem. Soc.*, 2016, **138**, 9301–9307.
75 O. Shekhah, Y. Belmabkhout, Z. Chen, V. Guillerm, A. Cairns, K. Adil and M. Eddaoudi, *Nat. Commun.*, 2014, **5**, 4228.
76 W. L. Queen, M. R. Hudson, E. D. Bloch, J. A. Mason, M. I. Gonzalez, J. S. Lee, D. Gygi, J. D. Howe, K. Lee, T. A. Darwish, M. James, V. K. Peterson, S. J. Teat, B. Smit, J. B. Neaton, J. R. Long and C. M. Brown, *Chem. Sci.*, 2014, **5**, 4569–4581.
77 J. Hoffman, L. Proaño and C. W. Jones, *ACS Appl. Polym. Mater.*, 2025, **7**, 15671–15681.
78 Z. Zhu, H. Tsai, S. T. Parker, J. Lee, Y. Yabuuchi, H. Z. Jiang, Y. Wang, S. Xiong, A. C. Forse and B. Dinakar, *J. Am. Chem. Soc.*, 2024, **146**, 6072–6083.
79 W. Wei, Z. Wang, C. Xu, Z. Li, H. Bai and Z. Liu, *Ind. Eng. Chem. Res.*, 2025, **64**, 24276–24299.
80 H. Daglar, Z. Zhou, R. Zhu, P. Parihar, J. I. Siepmann, O. M. Yaghi and L. Gagliardi, *J. Am. Chem. Soc.*, 2025, **148**(1), 1614–1622.
81 M. Fayaz and A. Sayari, *ACS Appl. Mater. Interfaces*, 2017, **9**, 43747–43754.
82 A. Sinha, L. A. Darunte, C. W. Jones, M. J. Realff and Y. Kawajiri, *Ind. Eng. Chem.*, 2017, **56**, 750–764.
83 I. Nicotera, A. Enotiadis and C. Simari, *Small*, 2024, **20**, 2401303.
84 J. L. Wade, H. L. Marques, W. Wang, J. Flory and B. D. Freeman, *J. Membr. Sci.*, 2023, **685**, 121954.
85 I. S. Metcalfe, G. A. Mutch, E. I. Papaioannou, S. Tsochataridou, D. Neagu, D. J. L. Brett, F. Iacoviello, T. S. Miller, P. R. Shearing and P. A. Hunt, *Nat. Energy*, 2024, **9**, 1074–1083.
86 T. Wang, K. S. Lackner and A. B. Wright, *Phys. Chem. Chem. Phys.*, 2013, **15**, 504–514.
87 C. Wu, Q. Huang, Z. Xu, A. T. Sipra, N. Gao, L. P. d. S. Vandenberghe, S. Vieira, C. R. Soccol, R. Zhao, S. Deng, S. K. S. Boetcher, S. Lu, H. Shi, D. Zhao, Y. Xing, Y. Chen, J. Zhu, D. Feng, Y. Zhang, L. Deng, G. Hu, P. A. Webley, D. Liang, Z. Ba, A. Mlonka-Mędrala, A. Magdziarz, N. Miskolczi, S. Tomasek, S. S. Lam, S. Y. Foong, H. S. Ng, L. Jiang, X. Yan, Y. Liu, Y. Ji, H. Sun, Y. Zhang, H. Yang, X. Zhang, M. Sun, D. C. W. Tsang, J. Shang, C. Muller, M. Rekhtina, M. Krödel, A. H. Bork, F. Donat, L. Liu, X. Jin, W. Liu, S. Saqline, X. Wu, Y. Xu, A. L. Khan, Z. Ali, H. Lin, L. Hu, J. Huang, R. Singh, K. Wang, X. He, Z. Dai, S. Yi, A. Konist, M. H. S. Baqain, Y. Zhao, S. Sun, G. Chen, X. Tu, A. Weidenkaff, S. Kawi, K. H. Lim, C. Song, Q. Yang, Z. Zhao, X. Gao, X. Jiang, H. Ji, T. E. Akinola, A. Lawal, O. S. Otitoju, M. Wang, G. Zhang, L. Ma, B. C. Sempuga, X. Liu, E. Oko, M. Daramola, Z. Yu, S. Chen, G. Kang, Q. Li, L. Gao, L. Liu and H. Zhou, *Carbon Capture Sci. Technol.*, 2024, **11**, 100178.
88 Y. Zhao and W. W. Ho, *J. Membr. Sci.*, 2012, **415**, 132–138.
89 J. S. Schultz, J. D. Goddard and S. R. Suchdeo, *AIChE J.*, 1974, **20**, 417–445.
90 Y. Han and W. S. W. Ho, *Ind. Eng. Chem.*, 2020, **59**, 5340–5350.
91 H. Xu, S. G. Pate and C. P. O'Brien, *Chem. Eng. J.*, 2023, **460**, 141728.
92 X. Deng, C. Zou, Y. Han, L. Lin and W. W. Ho, *J. Phys. Chem. C*, 2020, **124**, 25322–25330.
93 C. Zou, X. Deng, Y. Han and L.-C. Lin, *J. Phys. Chem. C*, 2025, **129**, 9550–9561.
94 H. Xu, S. G. Pate and C. P. O'Brien, *J. Membr. Sci.*, 2024, **689**, 122163.

95 Y. Zhao, Z. Wan, Z. Feng, D. Yang, Y. Zhang and F. Qu, *Int. J. Rock Mech. Min. Sci.*, 2012, **52**, 132–138.
96 E. Cussler, R. Aris and A. Bhown, *J. Membr. Sci.*, 1989, **43**, 149–164.
97 Z. Zhang, S. Rao, Y. Han, R. Pang and W. S. W. Ho, *J. Membr. Sci.*, 2021, **638**, 119696.
98 J. Zou and W. S. W. Ho, *J. Membr. Sci.*, 2006, **286**, 310–321.
99 R. Quinn and D. V. Laciak, *J. Membr. Sci.*, 1997, **131**, 49–60.
100 M. Sandru, T. Kim and M.-B. Hägg, *Desalination*, 2009, **240**, 298–300.
101 Y. Chen and W. S. W. Ho, *J. Membr. Sci.*, 2016, **514**, 376–384.
102 Y. Yuan, Z. Qiao, J. Xu, J. Wang, S. Zhao, X. Cao, Z. Wang and M. D. Guiver, *J. Membr. Sci.*, 2021, **620**, 118923.
103 Z. Dai, J. Deng, L. Ansaloni, S. Janakiram and L. Deng, *J. Membr. Sci.*, 2019, **578**, 61–68.
104 Z. Qiao, S. Zhao, M. Sheng, J. Wang, S. Wang, Z. Wang, C. Zhong and M. D. Guiver, *Nat. Mater.*, 2019, **18**, 163–168.
105 S. Li, Z. Wang, X. Yu, J. Wang and S. Wang, *Adv. Mater.*, 2012, **24**, 3196–3200.
106 L. Ansaloni, Y. Zhao, B. T. Jung, K. Ramasubramanian, M. G. Baschetti and W. S. W. Ho, *J. Membr. Sci.*, 2015, **490**, 18–28.
107 S. Cong, Q. Shen, M. Shan, J. Wang, J. Liu and Y. Zhang, *Chem. Eng. J.*, 2020, **383**, 123137.
108 S. Saqib, S. Rafiq, N. Muhammad, A. L. Khan, A. Mukhtar, S. Ullah, M. H. Nawaz, F. Jamil, C. Zhang and V. Ashokkumar, *J. Hazard. Mater.*, 2021, **411**, 125155.
109 Y. Pu, Z. Yang, V. Wee, Z. Wu, Z. Jiang and D. Zhao, *J. Membr. Sci.*, 2022, **641**, 119912.
110 J. Lu, X. Zhang, L. Xu, G. Zhang, J. Zheng, Z. Tong, C. Shen and Q. Meng, *Membranes*, 2021, **11**, 35.
111 X. Lu, J. Wang, Y. Wang and X. Zhang, *Sep. Purif. Technol.*, 2025, **358**, 130380.
112 B. Comesaña-Gándara, J. Chen, C. G. Bezzu, M. Carta, I. Rose, M.-C. Ferrari, E. Esposito, A. Fuoco, J. C. Jansen and N. B. McKeown, *Energy Environ. Sci.*, 2019, **12**, 2733–2740.
113 L. M. Robeson, *J. Membr. Sci.*, 2008, **320**, 390–400.
114 K. Ghosal, R. Chern, B. Freeman, W. Daly and I. Negulescu, *Macromolecules*, 1996, **29**, 4360–4369.
115 K. Ghosal, R. T. Chern, B. D. Freeman, W. H. Daly and I. I. Negulescu, *Macromolecules*, 1996, **29**, 4360–4369.
116 L. Zhu, D. Tian, D. Shin, W. Jia, C. Bae and H. Lin, *J. Polym. Sci., Part B: Polym. Phys.*, 2018, **56**, 1239–1250.
117 Y. Long, J. Jiang, J. S. Smink, J. E. ten Elshof, W. Rohlfs, C. W. Visser and W. Brilman, *Results Eng.*, 2025, **26**, 104766.